

Article

Investigation of the Effect of Laser Fluence on Microstructure and Martensitic Transformation for Realizing Functionally Graded NiTi Shape Memory Alloy via Laser Powder Bed Fusion

Paola Bassani, Jacopo Fiocchi , Ausonio Tuissi and Carlo Alberto Biffi * 

National Research Council of Italy, Institute of Condensed Matter Chemistry and Technologies for Energy, Unit of Lecco, CNR ICMATE, Via Previati 1/E, 23900 Lecco, Italy

* Correspondence: carloalberto.biffi@cnr.it; Tel.: +39-03412350111

Abstract: Nowadays, additive manufacturing (AM) of NiTi shape memory alloy is a challenging topic for the realization of 3D functional parts. Particularly, Laser Powder Bed Fusion (LPBF) of NiTi powder is one of the most challenging processes belonging to AM, thanks to its best performances in terms of productivity and precision of geometrical complexity. The control of the functional performances in NiTi components requires a strong interaction between technological and metallurgical approaches. In fact, a strong correlation among the process conditions, the microstructure, and the final functional performances, beyond the defects associated with the process are needed to be understood and analyzed. In the present work, the correlation between the feasibility map of processability and the obtained microstructure, which can be tailored according to the use of different energy density values, of Ni-rich NiTi powder processed with LPBF is investigated. In detail, discrete energy density values, in the range 60–300 J/mm³, were correlated to microstructure, Ni:Ti ratio, and transformation temperatures of the martensitic transformation, analyzed with SEM, EBSD, EDX, and DSC characterizations, respectively. An increase in laser energy density was found to promote Ni evaporation, which induced a change of the microstructure from austenite to martensite at room temperature. A consequent shift of the transformation temperatures to higher values and a change in microstructural texture was achieved. These achievements can support the identification of the feasibility range for manufacturing functionally graded NiTi SMA, requiring tailored functional properties located in selected positions in the 3D parts.



Citation: Bassani, P.; Fiocchi, J.; Tuissi, A.; Biffi, C.A. Investigation of the Effect of Laser Fluence on Microstructure and Martensitic Transformation for Realizing Functionally Graded NiTi Shape Memory Alloy via Laser Powder Bed Fusion. *Appl. Sci.* **2023**, *13*, 882. <https://doi.org/10.3390/app13020882>

Academic Editors: Ana M. Camacho and Mehrshad Mehrpouya

Received: 8 November 2022

Revised: 12 December 2022

Accepted: 23 December 2022

Published: 9 January 2023



Copyright: © 2023 by the authors. Licensee MDPI, Basel, Switzerland. This article is an open access article distributed under the terms and conditions of the Creative Commons Attribution (CC BY) license (<https://creativecommons.org/licenses/by/4.0/>).

Keywords: NiTi; shape memory alloy laser powder bed fusion; microstructure; EBSD; martensitic transformation

1. Introduction

Among Shape Memory Alloys (SMAs), intermetallic near equiatomic NiTi compound is the most diffused and well-known smart metallic material, which can offer unique properties, among which the more characteristic are shape memory effect (SME) and pseudoelasticity (PE) [1]. These peculiar characteristics depend on a diffusionless phase transformation occurring in the solid state, namely martensitic transformation (MT), which occurs, to a first approximation, above room temperature in Ti-rich NiTi, and below room temperature in Ni-rich NiTi alloys [2]. Transformation temperatures of the MT and stable, functional characteristics are strongly affected not only by Ni/Ti ratio but also by microstructural features such as grain size, texture, and eventual secondary phases or precipitates. All these features are intimately related to the thermal history of the material during production: this correlation imposes a strict control of the manufacturing parameters for fixing the final functional performances of NiTi SMA parts [3,4].

In the last years, the most studied advanced manufacturing process of NiTi SMA has been 3D printing, or additive manufacturing (AM), which is able to offer flexibility in designing complex structures integrating the functional performances of this smart

material [5–7]. Literature reports several scientific works regarding significant issues to be taken into account, including Ni loss [8], suitable heat treatments [9], and functional performance optimization of the parts [10]. The most diffused and investigated AM process is the Laser Powder Bed Fusion (LPBF) or Selective Laser Melting (SLM). Other relatively new metal additive manufacturing methods, such as Wire Arc Additive Manufacturing (WAAM) process, have the advantage of higher deposition rates and the capability of producing larger components but suffer from lower accuracy [11–13]. Thus, LPBF or SLM can offer much superior accuracy and greater flexibility in geometry design. In this process, a high-power laser beam melts a portion of the powder bed locally: this indicates very high cooling rates can be achieved, provoking the generation of fine and oriented grains. Anyways, due to high thermal gradients induced by the laser beam scans, some local chemical inhomogeneities can also be another typical issue of the SLM process.

The literature provides several works focused on processability, microstructure, and functional properties of additive manufactured samples produced using Ni-rich NiTi and Ti-rich NiTi powders, specifically for biomedical and aerospace applications. A common finding is that MT temperatures comparable to those of the wrought alloy can be obtained [1–15]; at the same time, the modulation of MT through a strict Ni/Ti ratio control reveals to be a challenging issue [16,17]. SLMed and wrought NiTi also differ in other relevant issues: different texture orientations are generally observed, and local chemical compositions which arise from the manufacturing process characteristics, such as cooling rates and thermal gradients [18], proved to be critical for the former. The NiTi-built microstructure can be strongly textured due to the evident epitaxial grain growth, oriented along the building direction [19]. The obtained microstructure is able to tailor the functional properties, as reported in several works [20–22]. The usable incident laser fluence range can induce different cooling rates and modified melt pool sizes, which are able to induce the formation of microstructures exhibiting different levels of texturing. Indeed, most of the reported literature works make use of lasers working in continuous mode, limited laser fluence variation is considered, and comparison of works from different research groups can be difficult due to varied initial powder composition of ancillary production conditions. As a result, still, some aspects of the correlation between the process parameters and the microstructure and chemical composition are not completely understood, especially for pulsed laser processes, for which reported data are clustered around the lowest fluence values that guarantee sufficient high relative density in the produced specimen.

More specifically oriented to novel achievements in the use of NiTi powders processed by AM, the realization of functionally graded NiTi samples, in which the adjustment of the process parameters was carried out with the goal of changing the chemical composition, was recently studied [23]. By promoting a variation of the Ni:Ti ratio, a Ti-rich NiTi layer can be obtained starting from Ni-rich NiTi powder, inducing a variation of the corresponding functional behavior. In this work, only two blocks with fully SE and SME behaviors overlapped each other and were realized with a different set of process parameters.

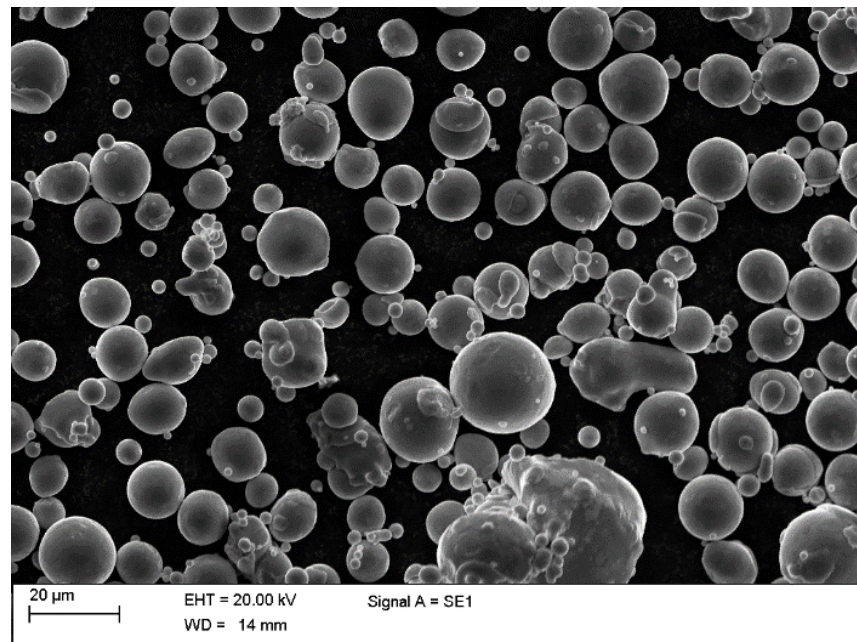
In this context, the present work has the scope of exploring the evolution of microstructure, chemical composition, and martensitic transformation of NiTi samples built with a wide range of laser fluence, obtained with different sets of process parameters, selected for achieving almost full dense samples. These achievements can be useful for realizing functionally graded NiTi parts, having gradients of functional performances.

2. Materials and Methods

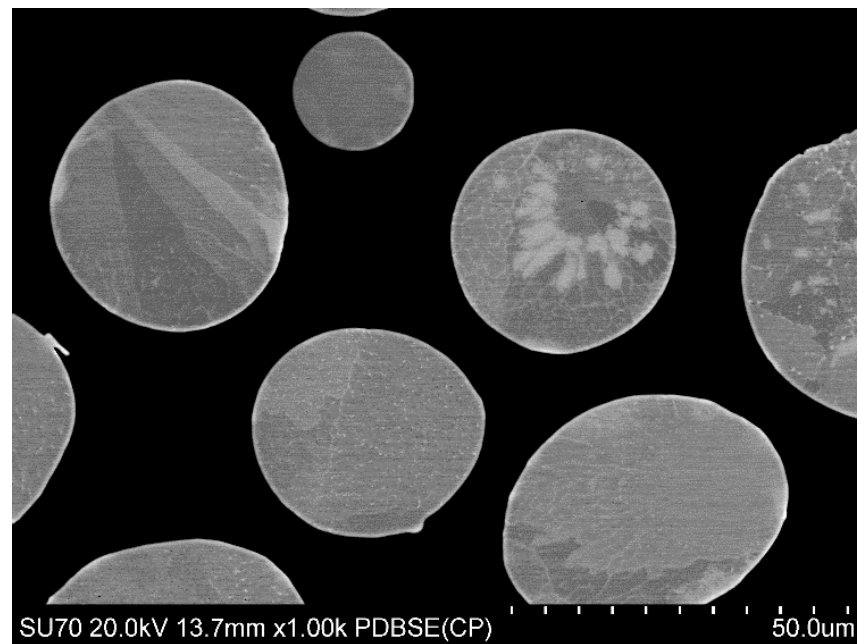
2.1. Material

The shape memory alloy considered in the present work is a Ni-rich NiTi, with composition of Ni_{50.8}Ti_{49.2} (at.%). The material was provided in the form of rather spherical powder (see Figure 1), having a size approximately in the range 5–50 μm. BackScatter Electron micrographs of powder cross-section evidenced typical microstructure of atomized materials, with dendritic structures and segregations. DSC measurement evidenced the

presence of MT below room temperature (see Figure 2); width of the peak can be related to chemical inhomogeneity and residual stresses due to atomization process.

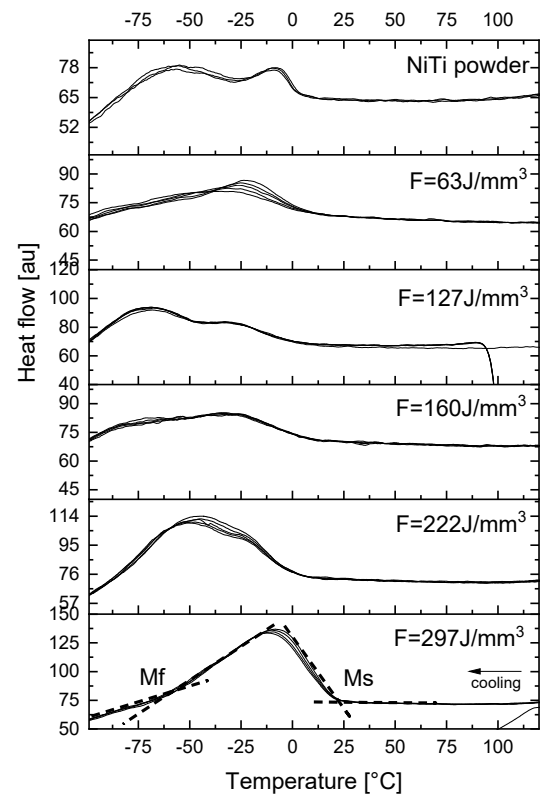


(a)

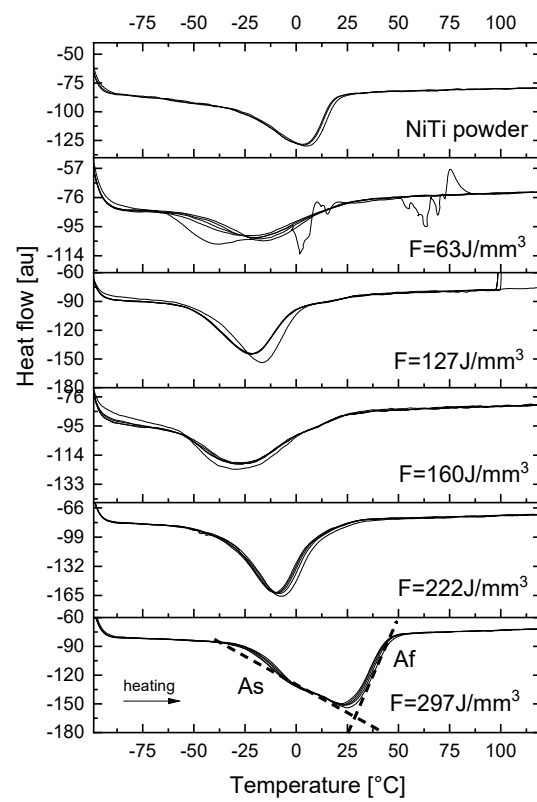


(b)

Figure 1. SEM image of the NiTi powder used for the LPBF process (a) overview of the powder shape (secondary electron micrograph), (b) powder section (Backscatter electron micrograph).



(a)



(b)

Figure 2. DSC measures of the initial NiTi powder and the NiTi samples, produced at varying the laser fluence. The DSC scans were splitted in cooling (a) and heating (b), respectively; tangent lines to the DSC profiles for detecting the transformation temperatures are depicted.

2.2. Laser Powder Bed Fusion Process

An SLM system (mod. AM400 from Renishaw) was used to produce cylindrical samples (3 mm in diameter, 5 mm in height). The system is equipped with a pulsed wave laser with a maximum power of 400 W. From a previous work [24,25], the feasibility area of processability was studied in the range of laser fluence 60–300 J/cm³. A wide range of process parameters was taken into account for the realization of the NiTi samples, printed on a Ti6Al4V platform at room temperature. Typical variation of density with laser fluence was observed, with initially steep increasing density values, then a rather wide plateau followed by a gentle decrease. Among the numerous specimens, a selection of five specimens was highlighted, characterized by high density and very different fluence values. The adopted process parameters are listed in Tables 1 and 2, together with the corresponding relative density values, measured via Archimede's method.

Table 1. List of variable process parameters used for the printing NiTi cylinders.

Power [W]	Exposure Time [μs]	Fluence [J/mm ³]	Relative Density [%]
30	125	63	97.7
75	100	127	98.4
125	75	160	99.9
175	75	222	99.2
175	100	297	98.3

Table 2. List of fixed process parameters used for printing the NiTi cylinders.

Parameters	Values
Scanning strategy	Meander
Atmosphere	Argon
Layer thickness	30 μm
Hatch distance	50 μm
Point distance	50 μm
Laser spot size	65 μm
Oxygen level	<20 ppm

The determination of the fluence, incident on the single powder bed, can be carried out as follows (see Equation (1)):

$$F = \frac{P \cdot t_{\text{exp}}}{d_p \cdot d_h \cdot t} \quad (1)$$

where P , t_{exp} , d_p , d_h and t indicate the laser power, the exposition time, the point distance, the hatch distance and the layer thickness, respectively.

2.3. Sample Characterizations

Relative density was derived, with the Archimedes method, on all the SLMed samples. Measurements were performed with a Gibertini E 50 S/2 balance equipped with a setup for density measurement purposes. The details of the relative density results are reported elsewhere [25].

Calorimetric properties of the SLMed NiTi samples were investigated through a differential scanning calorimeter (DSC, mod. SSC 5200 by Seiko Instruments), in the [−100 °C; 150 °C] range with heating/cooling rate of 10 °C min. Characteristic temperatures and corresponding transformation enthalpies were evaluated for both direct/reverse transformations upon cooling/heating at the second thermal cycle.

Microstructural investigations were mainly conducted with Scanning Electron Microscopy (SEM). To derive texture information, Electron Back Scatter Diffraction (EBSD) analyses were performed, while average qualitative composition was obtained with Energy Dispersive X-ray Spectroscopy (EDXS) on the xz views (orthogonal to the building platform) for the five selected samples (FEG-SEM mod. SU70 from Hitachi, EBSD and EDX

from ThermoFisher Scientific, Waltham, MA, USA). Sectioned specimens were included in graphite-loaded hot mounting resin, and after conventional metallographic preparation, a final polishing step with colloidal silica was applied.

3. Results

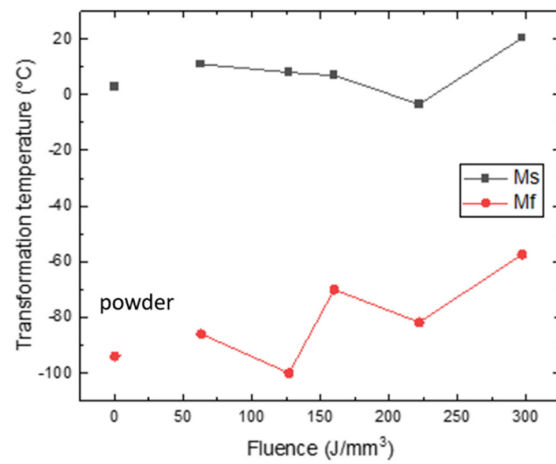
The investigated process conditions were selected according to two criteria: significant distance in fluence values and the highest density (among the samples processed with different processing parameters that provide similar fluence). The laser fluence values ranged from 63 J/mm³ up to 297 J/mm³ (see Table 1); these values fit well with the indications achievable from the literature regarding the processability of NiTi SMA powder through the PBPF process [26].

In Figure 2, the evolution of the martensitic transformation (MT) of the initial NiTi powder and the NiTi-built samples, produced at varying laser fluence, is depicted. Each sample was analyzed with three complete heating/cooling cycles in the DSC scans. It can be recognized that all the analyzed samples exhibit the peaks of the martensitic transformation and good overlapping of the DSC signals, indicating good thermal stability of the martensitic transformation.

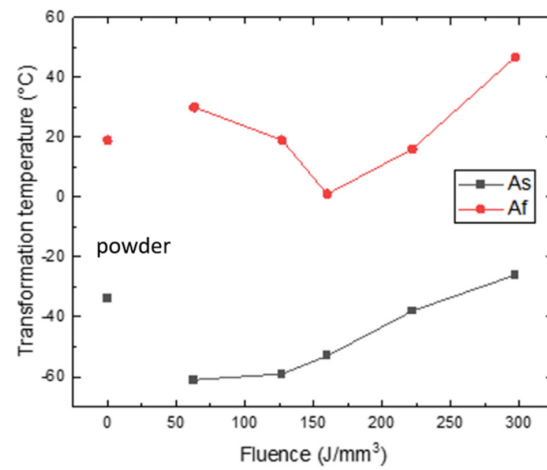
In detail, the initial powder shows a multistage phase transformation upon cooling, which can be associated with chemical inhomogeneities and residual stresses formed during the gas atomization process, as confirmed by BSE micrographs of powders (Figure 1). The corresponding transformation temperatures, measured at the second DSC cycle and plotted in Figure 3, confirm that the NiTi powder is austenitic at room temperature (25 °C). The sample built at the lowest fluence shows a broad single-stage transformation upon both heating and cooling. By increasing the laser fluence in the building of NiTi samples, it can be observed that the direct martensitic transformation tends to evolve to a better-defined but still broad transformation peak, with two-stage transformation upon cooling and increasing transformation temperatures. The sample built with the highest fluence, conversely to all other specimens, shows a two-stage transformation upon heating, definitely shifted to a temperature higher than room temperature, as depicted in Figure 3.

In particular, martensite start (Ms) and finish (Mf) temperatures and the austenite start (As) and finish (Af) temperatures are plotted in Figure 3a,b, respectively. It was found that Ms decreased from 10 °C down to 0 °C upon increasing the laser fluence from 63 up to 222 J/mm³, while it increased up to 20 °C at 297 J/mm³. The trend of Mf was associated with some oscillations, due also to the sluggish shape of the peaks, that hinder a precise determination of start and finish temperatures. Nether the less, a tendency trend can be marked, suggesting an increase in the Mf from low to high laser fluence up to −55 °C. Regarding the reverse martensitic transformation, As was almost constant (−60 °C) in the range 63–127 J/mm³, while it increased significantly up to −25 °C; on the contrary, Af decreased from 30 °C down to 0 °C in the range 63–160 J/mm³, then it started to increase up to 50 °C as well.

Figure 4 shows the trend of the transformation enthalpies upon heating and cooling obtained from the DSCs of the fabricated NiTi samples. The enthalpy values of the direct and reverse martensitic transformation of the initial powder were 8 J/g and 7 J/g, respectively. These values are largely lower than the typical ones of the cast and heat-treated NiTi SMAs, reasonably due to chemical inhomogeneity and residual stress left from the atomization process. Regarding the printed NiTi samples, the enthalpies of both the direct and reverse martensitic transformation showed the same trend: they increased from 5 J/g, obtained in correspondence with the lowest laser fluence, up to 13 J/g and 19 J/g, respectively, at the highest fluence value. These latter values are closer to the average values of transformation enthalpies for cast NiTi SMAs [27].



(a)



(b)

Figure 3. Evolution of the transformation temperatures of the direct (a) and reverse (b) martensitic transformation of the initial NiTi powder and the NiTi samples, produced at varying the laser fluence.

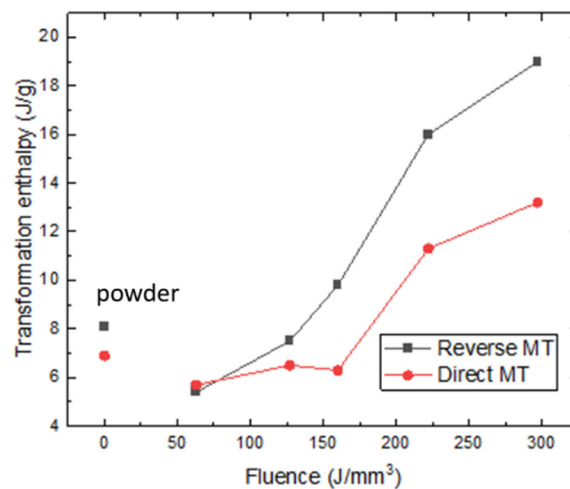


Figure 4. Evolution of the transformation enthalpies of the direct and reverse martensitic transformation of the NiTi powder and the NiTi samples, produced at varying the laser fluence.

EDXS measurements were performed on XZ sections of the as-built samples; nine area measurements of about $0.5 \times 0.5 \text{ mm}^2$ were acquired for each specimen, spread over a total area of about $2.5 \times 2 \text{ mm}$. Figure 5 shows the semiquantitative trend of Ni and Ti content, expressed in atomic percentage (at. %), at varying laser fluence.

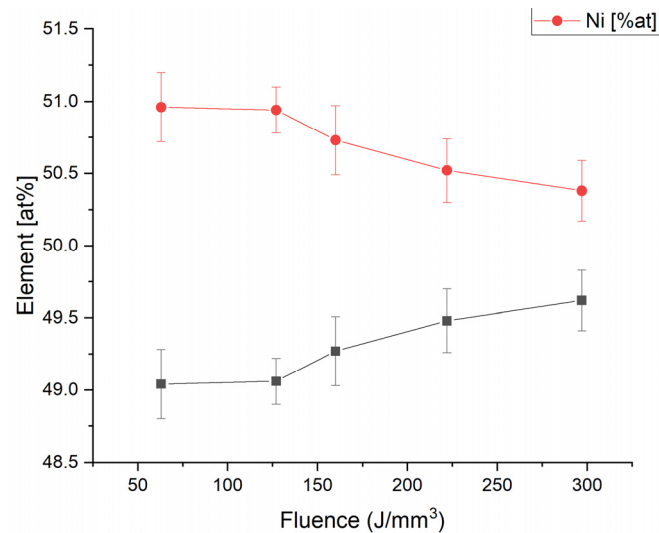


Figure 5. Compositional analysis, carried out with EDS, of the NiTi built samples processed at different laser fluence values.

No significant O content was observed, without any variation among the position in the specimens; consequently, it was disregarded from calculations. In the graph, two regions can be clearly observed; at low laser fluence values up to 63–160 J/mm³, the compositions of the specimens are quite constant and in good agreement with the nominal composition of the starting powder, i.e., Ni content of about $51.0 \pm 0.3 \text{ at. } \%$, quite close to the nominal 50.8%at. By increasing further the laser fluence, up to 297 J/mm³, Ni content decreased down to $50.4 \pm 0.2 \text{ at. } \%$, with a consequent increase in Ti content, was detected from $49.0 \pm 0.3 \text{ at. } \%$ up to $49.6 \pm 0.2 \text{ at. } \%$. The latter values are well in agreement with the observed increase in the transformation temperature in DSC analyses.

EBSD analyses were carried out in as-built conditions at room temperature. Figure 6 shows the evolution of the orientation imaging microscopy (OIM), inverse pole figures (IPF), and calculated (100) pole figures of the samples sectioned along the Z direction, i.e., the building direction (orthogonal to the platform). It can be seen that the PW laser emission mode can induce a significant variation of the microstructure and crystallographic texture at varying laser fluence. The samples, processed with laser fluence up to 160 J/mm³, exhibit a full austenitic phase, as shown in Figure 6a–c; at 222 J/mm³, the sample shows small areas not recognized by EBSD as austenite; therefore, traces of martensite can be indirectly identified (see Figure 6d). At the highest value of laser fluence (297 J/mm³), during the first analysis, most of the analyzed area could not be recognized by EBSD and exhibited very low pattern quality. After a thermal cycle (heating with hot water, then cooling again to room temperature), EBSD analysis was repeated (Figure 6e); still, some areas were nonindexed as observable, but most of the specimen was indexed as austenite; the nonindexed regions in the first analyses were clearly related to the region of the samples in which martensite could be easily formed upon cooling during specimen preparation, by washing with too cold tap water, that easily transformed back upon moderate heating. Indeed DSC analyses show that Martensite formation started at about 20 °C. The other nonindexed regions can be ascribed hence at chemical inhomogeneity or residual stresses-retained martensite [28].

Change in the microstructure of the specimen can be clearly seen from OIM: at low fluence values, a rather homogenous microstructure is observed, characterized by small grains, while at increasing fluence, a coarser microstructure can be observed, characterized by bands parallel to the Z direction, composed by columnar grains.

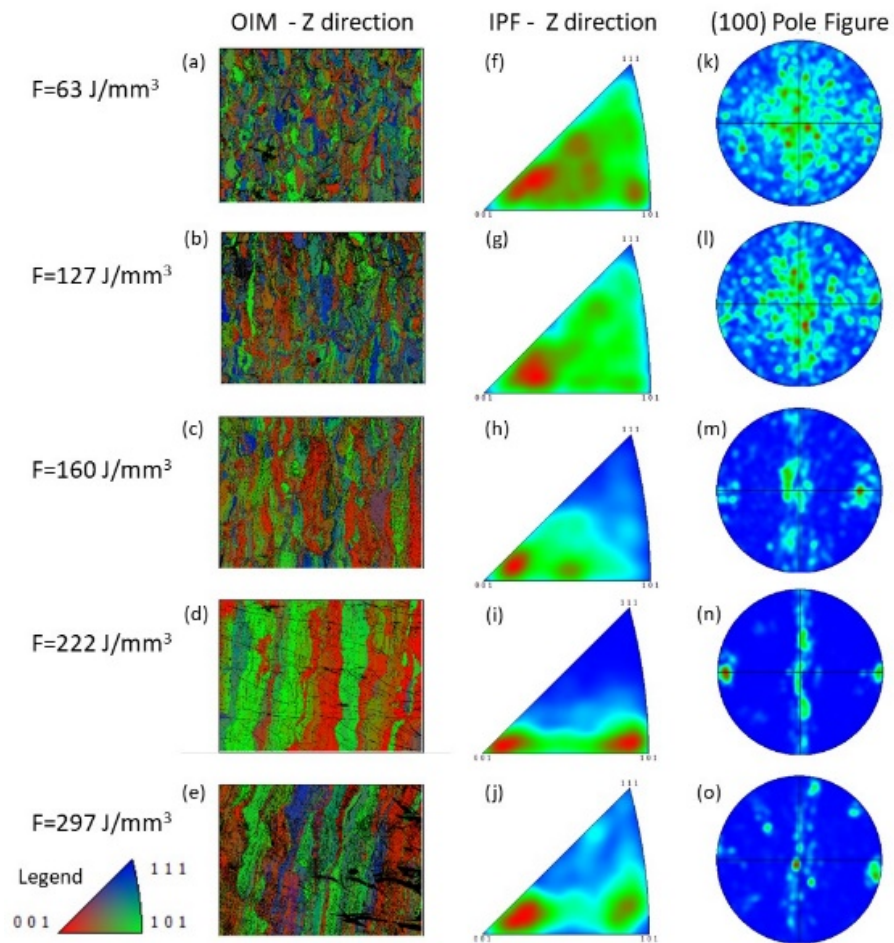


Figure 6. Texture information derived from EBSD analyses of xz section of NiTi samples manufactured upon increasing the laser fluence: orientation imaging microscopy (a–e), inverse pole figures (f–j) according to Z direction, i.e., Building Direction (vertical in the section) and (100) calculated pole figures (k–o).

In Figure 7, the pattern quality maps of small areas of the analyzed surfaces are reported; in order to highlight melt pool shape and size, red lines were added to representative melt pool boundaries to guide the eyes. At the lowest value of laser fluence (63 J/mm^3), rather small semi-spherical liquid pools are generated. At increasing fluence rate, melt pools widen both laterally and in-depth; extensive remelting occurs, especially on the sides of the melt pools. Concurrently, in the smaller melt pools, both grains extend from one boundary to another, and smaller grains contained inside the melt pool can be observed. At the higher fluences, almost only columnar grains can be noticed, thinner and thinner, with several of them sharing similar orientations.

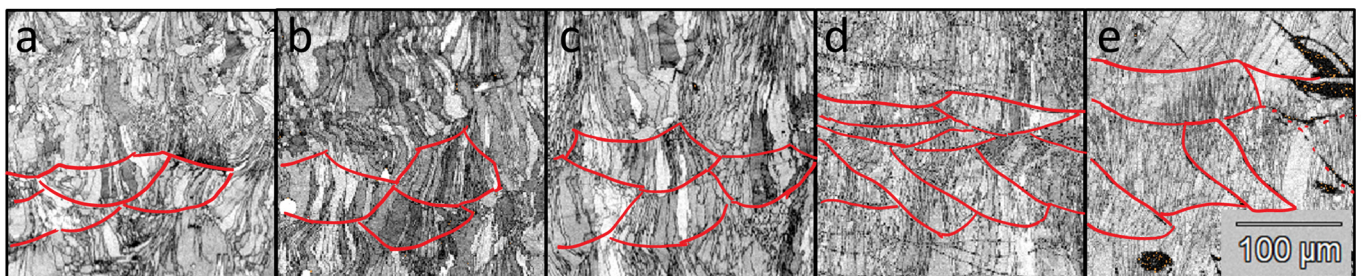


Figure 7. EBSD analyses on xz section of NiTi specimens; pattern quality maps, with outlined some representative melt pool boundaries (a–e); increasing fluence.

From the analysis of IPF and PF, it can be stated that the change in the morphology of the microstructure is also combined with a corresponding modification of crystallographic texture; at 63 J/mm^3 , no evident preferred orientation of the texture can be detected from the EBSD investigation (see Figure 6f,k) along the (001) orientation.

By increasing the laser power density and the overheating of the melt pools, columnar to cellular/planar grain growth is favored instead of dendritic and equiaxed ones. Moreover, also epitaxial growth is favored. As depicted in Figure 6g,l, just a few epitaxial grains can be observed at 127 J/mm^3 , and this trend becomes more and more evident with increasing the laser fluence from 160 J/mm^3 up to 297 J/mm^3 ; under these conditions, grains nucleates in melt pool and grew through several building layers. The texture orientation remains mainly oriented to (001) under irradiation up to 160 J/mm^3 ; on the contrary, higher laser fluence (i.e., 222 J/mm^3) induced a double preferential orientation of the microstructural texture along both (001) and (101) orientations. This change in texture does not correlate with DSC results; the orientation of a grain does not change the MT heat effect but is extremely important for mechanical properties and MT effects such as SMA and SE effects [18].

Finally, a relevant amount of martensite was detected at the highest value of laser fluence (297 J/mm^3). This was also observed in the manufacturing of NiTi lattice structures [28], in which martensite could be induced by a change of chemical composition, in terms of Ni:Ti ratio, or induced by residual stress, which may be promoted by the large thermal gradients.

It is worth to be noticed that the border of the liquid pools, in correspondence with 222 J/mm^3 and 297 J/mm^3 , are more clearly visible, as shown in Figure 7, due to a wider region of not indexed point, with respect to grain boundaries. It can probably be assumed that the border of the laser tracks is decorated by martensite. As a justification of this behavior, it can be seen that by increasing the laser fluence up to 297 J/mm^3 , the generation of martensite is largely promoted (see Figure 7e).

4. Discussion

The increase in the laser fluence can dramatically change the microstructural features of the laser-melted NiTi SMA. As depicted in Figure 6, the evolution of the microstructure suggested a change in the solidification conditions, as can be observed by the passage from rather equiaxial small grains to bigger columnar grain growth oriented along the building direction. The marked difference in texture can be ascribed to geometrical constraints and changes in solidification structures. In detail, the equiaxial grains are associated with very quick cooling rates; in fact, under irradiation at limited laser fluence, the dimension of the liquid pool is small; therefore, the limited amount of liquid metal can experience fast cooling rates and consequent dendritic or columnar/dendritic grow. Fast cooling favors nucleation overgrowth from existing grains. On the contrary, high laser fluence can induce a larger amount of liquid material, requiring a longer time to be cooled and hence reduced, even if still high, cooling rates. As a result, in the latter process condition, the microstructure would be characterized by columnar grains that preferably grow epitaxially from existing grains along the direction of the thermal gradient. The latter can be assumed, as the first approximation, perpendicular to the melt pool boundary: at low fluence, melt pools are semicircular; hence, more growth direction can be experienced by the grains. At higher fluence, only the central part of the melt pools survives to subsequent melting passes; and they are aligned mostly parallel to the building plane. Consequently, grains with different growth directions are in less amount, as they were melted during subsequent steps. The different degrees of texture evidenced by the samples can be ascribed to the combination of different extend of epitaxial growth, combined with rotation at each pass of the laser scanning direction and different shape/remelted portions of melt pools.

The MT exhibits a modification of its transformation temperatures and enthalpies under the described increase in laser fluence, as depicted in Figures 2–4. In this case, an almost continuous decrease in the Ni content is directly associated with the increase in

the energy irradiated to the powder bed during the LPBF process; higher overheating temperatures are reasonably reached in the melt pool for longer times, promoting selective evaporation of Ni. This effect has already been observed for a similar process applied to NiTi SMAs [24,29]. Not only higher overheating of the melt occurs at higher fluence: the increased amount of transferred heat propagates to the previously built layers and promotes recovery and annealing phenomena in the heat-affected zones; this effect is witnessed by the increase in enthalpy at increasing fluence.

In fact, it is known that an excess laser fluence can typically induce porosity due to gas entrapment and potential local vaporization of elements. In particular, the presence of these defects can be explained by the energy required by the material to allow its melting and its partial vaporization, according to the following equation:

$$E = A \cdot \rho \cdot \{C_p \cdot [T_M - T_i] + L_M + m' \cdot L_V\}, \quad (2)$$

where A is the absorption coefficient; ρ is the density; C_p is the thermal capacity; T_M and T_i are the melting and initial temperatures, respectively; L_M and L_V are the latent heat of melting and vaporization, respectively; and m' represents the percentage of liquid material that is subjected to vaporization, if present during the laser irradiation.

In the case of laser fluence, just sufficient for inducing a proper melting of the powder bed, the term m' is equal to zero. On the contrary, if an excess of laser fluence is adopted during the SLM process, the parameter m' is higher than zero; therefore, vaporization can take place, having Ni at a higher vapor pressure than T_i . The peak of the relative density vs. laser fluence curve exhibits a compromise between the defects related to lack of fusion and gas porosities, as extensively discussed in the literature [28].

The schematic of the laser beam/material interaction during the powder scanning, representative of the two extreme conditions previously mentioned, is depicted in Figure 8 [30]. Under low laser fluence, limited penetration depth can be achieved (see Figure 8a), and the potentially associated defect is correlated to the lack of fusion due to insufficient energy irradiated from the laser beam. The fusion of the powder bed takes place, creating a stable and uniform path of the liquid pool.

On the contrary, upon an increase in the laser fluence, the penetration depth can be significantly increased, thanks to the vaporization of a limited amount of liquid metal (proportional to the coefficient m'), and the principal defect is related to the formation of spherical pores, due to the entrapment of the residual vaporized material (see Figure 8b).

It can be seen that from Figure 7, the shape and the size of the liquid pools versus the increase in the laser fluence follow the description suggested by Figure 8. In fact, low laser fluence (63 J/mm^3) induced a melting with limited depth, while the increase in fluence provoked a deeper liquid pool, also having an irregular shape.

The high fluence values can promote vaporization, leading not only to gas porosities but also to a possible compositional variation. This is in good agreement not only with the evolution of the Ni and Ti content versus the laser fluence, as shown in Figure 5, but also with the trend on the relative density, listed in Table 1. According to this, the transformation temperatures and the corresponding transformation enthalpies are subjected to a variation, which is due to the Ni content shift and to residual stresses, too.

The achieved results are also confirmed by a previous work, in which the laser parameters were varied with the aim of obtaining austenite or martensite in different portions of the same built sample. In that case, functionally graded NiTi SMAs were produced by the LPBF process by the local evaporation of Ni under the irradiation of the laser beam, incident under different energetic values [23]. The passage from martensite to austenite at room temperature becomes a potentiality for designing and producing functionally graded parts.

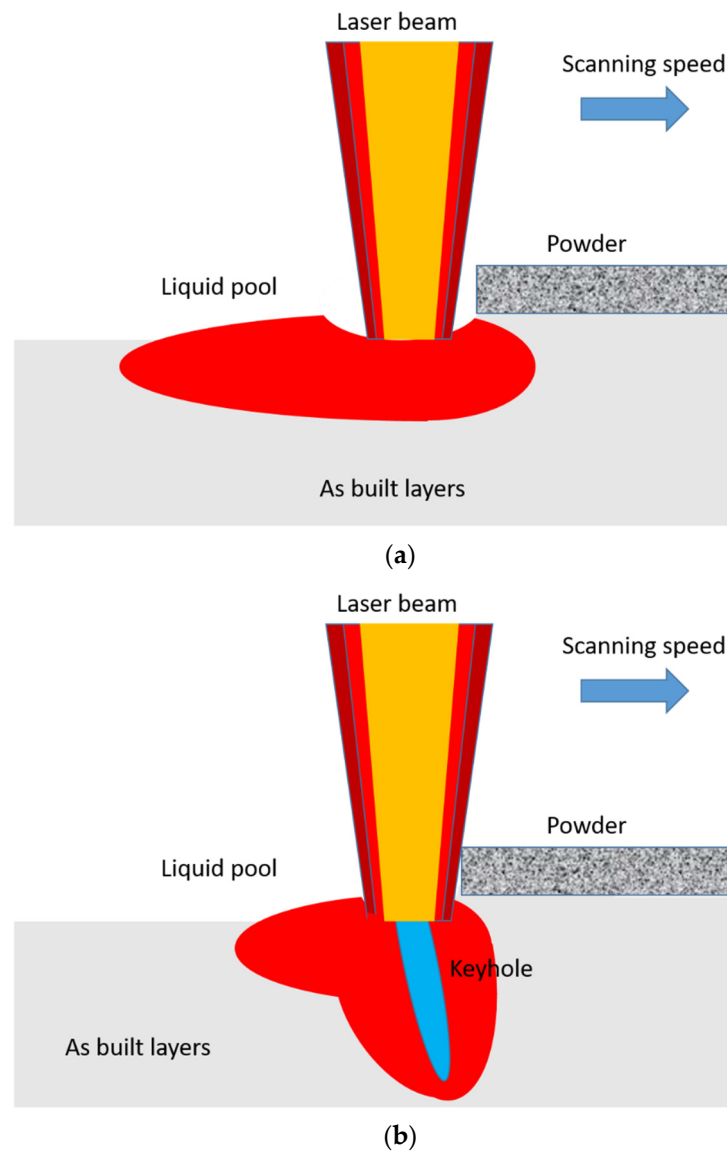


Figure 8. Schematic of the laser beam/ material interaction occurring at low (a) and high (b) laser fluence during the powder scanning [30].

5. Conclusions

The laser powder bed fusion process was used for producing fully dense or near full dense NiTi Shape Memory Alloy parts. The process parameters, including the laser power and the exposure time, were varied across a wide range. It was demonstrated that the variation of the laser power density in the range 63–297 J/mm³ could largely tune the Ni/Ti ratio due to the preferential Ni evaporation under the action of the laser beam; evident Ni loss up to 1% in atomic percentage was detected, resulting in an increase in the transformation temperatures of MT leading to Af from below room temperature, to higher than 40 °C. Moreover, it was found that low laser fluence can promote a rather equiaxed microstructure without a preferred orientation, while the increase in the laser fluence induced epitaxial growth of columnar grains aligned along the building direction, with preferred (100) or (101) orientation.

These results can be adopted for designing functionally graded NiTi structures, able to offer local PE or SME by controlling the evolution of the microstructure and chemical composition, or offering different mechanical performances, according to the degree and alignment of preferred texture.

Author Contributions: Conceptualization, P.B. and C.A.B.; methodology, C.A.B.; software, P.B.; validation, J.F. and P.B.; formal analysis, P.B. and C.A.B.; investigation, C.A.B. and P.B.; resources, A.T.; data curation C.A.B., P.B., J.F. and A.T.; writing—original draft preparation, C.A.B., P.B., J.F. and A.T.; writing—review and editing, C.A.B., P.B., J.F. and A.T.; visualization, C.A.B.; supervision, A.T. and C.A.B.; project administration, A.T.; funding acquisition, A.T. All authors have read and agreed to the published version of the manuscript.

Funding: This research received no external funding.

Institutional Review Board Statement: Not applicable.

Informed Consent Statement: Not applicable.

Data Availability Statement: Not applicable.

Acknowledgments: The authors acknowledge Saes Getters SpA as supplier of Nitinol powder. Further, the authors would like to thank N. Bennato from CNR ICMATE for his support in the specimen preparation.

Conflicts of Interest: The authors declare no conflict of interest.

References

- Funakubo, H. *Shape Memory Alloys*; Gordon and Breach Science Publishers: Amsterdam, The Netherlands, 1987.
- Nishida, M.; Wayman, C.; Honma, T. Precipitation processes in near-equiatomic TiNi shape memory alloys. *Metall. Mater. Trans.* **1986**, *17*, 1505–1515. [[CrossRef](#)]
- Elahinia, M.; Hashemi, M.; Tabesh, M.; Bhaduri, S.B. Manufacturing and processing of NiTi implants: A review. *Prog. Mater. Sci.* **2012**, *57*, 911–946. [[CrossRef](#)]
- Biffi, C.; Fiocchi, J.; Tuissi, A. Relevant aspects of laser cutting of NiTi shape memory alloys. *J. Mater. Res. Technol.* **2022**, *19*, 472–506. [[CrossRef](#)]
- Mitchell, A.; Lafont, U.; Holyńska, U.; Semprimoschnig, U. Additive manufacturing—A review of 4D printing and future applications. *Addit. Manuf.* **2018**, *24*, 606–626. [[CrossRef](#)]
- Elahinia, M.; Shayesteh Moghaddam, N.; Taheri Andani, M.; Amerinatanzi, A.; Bimber, B.A.; Hamilton, R.F. Fabrication of NiTi through additive manufacturing—A review. *Prog. Mater. Sci.* **2016**, *83*, 630–663. [[CrossRef](#)]
- Van Humbeeck, J. Additive Manufacturing of Shape Memory Alloys. *Shape Mem. Superelasticity* **2018**, *4*, 309–312. [[CrossRef](#)]
- Bormann, T.; Schumacher, R.; Müller, B.; Mertmann, M.; De Wild, M. Tailoring Selective Laser Melting Process Parameters for NiTi Implants. *J. Mater. Eng. Perform.* **2012**, *21*, 2519–2524. [[CrossRef](#)]
- Saedi, S.; Turabi, A.S.; Andani, M.T.; Haberland, C.; Karaca, H.; Elahinia, M. The influence of heat treatment on the thermomechanical response of Ni-rich NiTi alloys manufactured by selective laser melting. *J. Alloy. Compd.* **2016**, *677*, 204–210. [[CrossRef](#)]
- Shayesteh Moghaddam, N.; Saedi, S.; Amerinatanzi, A.; Hinojos, A.; Ramazani, A.; Kundin, J.; Mills, M.J.; Karaca, H.; Elahinia, M. Achieving superelasticity in additively manufactured NiTi in compression without post-process heat treatment. *Sci. Rep.* **2019**, *9*, 41. [[CrossRef](#)]
- Cooke, S.; Ahmadi, K.; Willerth, S.; Herring, R. Metal additive manufacturing: Technology, metallurgy and modelling. *J. Manuf. Process.* **2020**, *57*, 978–1003. [[CrossRef](#)]
- Çam, G. Prospects of producing aluminum parts by wire arc additive manufacturing (WAAM). *Mater. Today Proc.* **2022**, *62*, 77–85. [[CrossRef](#)]
- Xiong, Y.; Tang, Y.-L.; Zhou, Q.; Ma, Y.S.; Rosen, D.W. Intelligent additive manufacturing and design state of the art and future perspectives. *Addit. Manuf.* **2022**, *59*, 103139. [[CrossRef](#)]
- Saedi, S.; Moghaddam, N.S.; Amerinatanzi, A.; Elahinia, M.; Karaca, H.E. On the effects of selective laser melting process parameters on microstructure and thermomechanical response of Ni-rich NiTi. *Acta Mater.* **2018**, *14*, 552–560. [[CrossRef](#)]
- Speirs, M.; Wang, X.; Van Baelen, S.; Ahadi, A.; Dadbakhsh, S.; Kruth, J.P.; Van Humbeeck, J. On the Transformation Behavior of NiTi Shape-Memory Alloy Produced by SLM. *Shap. Mem. Superelasticity* **2016**, *2*, 310–316. [[CrossRef](#)]
- Shiva, S.; Palani, I.A.; Mishra, S.K.; Paul, C.P.; Kukreja, L.M. Investigation on the influence of composition in the development of Ni-Ti shape memory alloy using laser based additive manufacturing. *Opt. Laser Technol.* **2015**, *69*, 44–51. [[CrossRef](#)]
- Mahmoudi, M.; Tapia, G.; Franco, B.; Ma, J.; Arroyave, R.; Karaman, I.; Elwany, A. On the printability and transformation behavior of nickel-titanium shape memory alloys fabricated using laser powder-bed fusion additive manufacturing. *J. Manuf. Process.* **2018**, *35*, 672–680. [[CrossRef](#)]
- Nematollahi, M.; Saghaian, S.E.; Safaei, K.; Bayati, P.; Bassani, P.; Biffi, C.; Tuissi, A.; Karaca, H.; Elahinia, M. Building orientation-structure-property in laser powder bed fusion of NiTi shape memory alloy. *J. Alloy. Compd.* **2021**, *873*, 159791. [[CrossRef](#)]
- Bormann, T.; Müller, B.; Schinhammer, M.; Kessler, A.; Thalmann, P.; de Wild, M. Microstructure of selective laser melted nickel-titanium. *Mater. Charact.* **2014**, *94*, 189–202. [[CrossRef](#)]

20. Andani, M.T.; Saedi, S.; Turabi, A.S.; Karamooz, M.R.; Haberland, C.; Karaca, H.E.; Elahinia, M. Mechanical and Shape Memory properties of porous Ni_{50.1}Ti_{49.9} alloys manufactured by selective laser melting. *J. Mech. Behav. Biomed. Mater.* **2017**, *68*, 224–231. [[CrossRef](#)]
21. Moghaddam, N.S.; Saghaian, S.E.; Amerinatanzi, A.; Ibrahim, H.; Li, P.; Toker, G.P.; Karaca, H.E.; Elahinia, M. Anisotropic tensile and actuation properties of NiTi fabricated with selective laser melting. *Mater. Sci. Eng. A* **2018**, *724*, 220–230. [[CrossRef](#)]
22. Dadbakhsh, S.; Vrancken, B.; Kruth, J.P.; Luyten, J.; Van Humbeeck, J. Texture and anisotropy in selective laser melting of NiTi alloy. *Mater. Sci. Eng. A* **2016**, *650*, 225–232. [[CrossRef](#)]
23. Nematollahi, M.; Safaei, K.; Bayati, P.; Elahinia, M. Functionally graded NiTi shape memory alloy: Selective laser melting fabrication and multi-scale characterization. *Mater. Lett.* **2021**, *292*, 129648. [[CrossRef](#)]
24. Biffi, C.A.; Fiocchi, J.; Bassani, P.; Tuissi, A. Microstructure and Martensitic Transformation of Selective Laser Melted NiTi Shape Memory Alloy Parts. In Proceedings of the Second International Conference on Simulation for Additive Manufacturing (Sim-AM 2019), Pavia, Italy, 11–13 September 2019; ISBN 978-84-949194-8-0.
25. Biffi, C.A.; Fiocchi, J.; Valenza, F.; Bassani, P.; Tuissi, A. Selective Laser Melting of NiTi Shape Memory Alloy: Processability, Microstructure, and Superelasticity. *Shape Mem. Superelasticity* **2020**, *6*, 342–353. [[CrossRef](#)]
26. Haberland, C.; Elahinia, M.; Walker, J.M.; Meier, H.; Frenzel, J. On the development of high quality NiTi shape memory and pseudoelastic parts by additive manufacturing. *Smart Mater. Struct.* **2014**, *23*, 104002. [[CrossRef](#)]
27. Dadbakhsh, S.; Speirs, M.; Kruth, J.-P.; Schrooten, J.; Luyten, J.; Van Humbeeck, J. Effect of SLM Parameters on Transformation Temperatures of Shape Memory Nickel Titanium Parts. *Adv. Eng. Mater.* **2014**, *16*, 1140–1146. [[CrossRef](#)]
28. Biffi, C.A.; Bassani, P.; Fiocchi, J.; Tuissi, A. Microstructural and Mechanical Response of NiTi Lattice 3D Structure Produced by Selective Laser Melting. *Metals* **2020**, *10*, 814. [[CrossRef](#)]
29. Biffi, C.A.; Tuissi, A.; Demir, A.G. Martensitic transformation, microstructure and functional behavior of thin-walled Nitinol produced by micro laser metal wire deposition. *J. Mater. Res. Technol.* **2021**, *12*, 2205–2215. [[CrossRef](#)]
30. Liu, M.; Wei, K.; Yue, X.; Huang, G.; Deng, J.; Zeng, X. High power laser powder bed fusion of AlSi10Mg alloy: Effect of laser beam mode. *J. Alloy. Compd.* **2022**, *909*, 164779. [[CrossRef](#)]

Disclaimer/Publisher’s Note: The statements, opinions and data contained in all publications are solely those of the individual author(s) and contributor(s) and not of MDPI and/or the editor(s). MDPI and/or the editor(s) disclaim responsibility for any injury to people or property resulting from any ideas, methods, instructions or products referred to in the content.